Feel Yourself a Student!

Dear friends, I would like to give to you an interesting and reliable antenna theory. Hours searching in the web gave me lots theoretical information about antennas. Really, at first I did not know what information to chose for ANTENTOP. Finally, I stopped on lectures “Modern Antennas in Wireless Telecommunications” written by Prof. Natalia K. Nikolova from McMaster University, Hamilton, Canada.

You ask me: Why?

Well, I have read many textbooks on Antennas, both, as in Russian as in English. So, I have the possibility to compare different textbook, and I think, that the lectures give knowledge in antenna field in great way. Here first lecture “Introduction into Antenna Study” is here. Next issues of ANTENTOP will contain some other lectures.

So, feel yourself a student! Go to Antenna Studies!

I.G.

My Friends, the above placed Intro was given at ANTENTOP- 01- 2003 to Antennas Lectures.

Now I know, that the Lecture is one of popular topics of ANTENTOP. Every Antenna Lecture was downloaded more than 1000 times!

Now I want to present to you one more very interesting Lecture - it is a Lecture about Basic Methods in Antenna Measurements. I believe, you cannot find such info anywhere for free! Very interesting and very useful info for every ham, for every radio- engineer.

So, feel yourself a student! Go to Antenna Studies!

I.G.

McMaster University Hall

Prof. Natalia K. Nikolova

Basic Methods in Antenna Measurements

The basic concepts in antenna measurements are presented in this module. First, a brief description of antenna ranges and anechoic chambers is given. Second, the basic methods for measuring the far-field patterns, the gain, the directivity, the radiation efficiency, the impedance and the polarization are discussed.

by Prof. Natalia K. Nikolova

Basic Methods in Antenna Measurements

The basic concepts in antenna measurements are presented in this module. First, a brief description of antenna ranges and anechoic chambers is given. Second, the basic methods for measuring the far-field patterns, the gain, the directivity, the radiation efficiency, the impedance and the polarization are discussed.

1. Introduction

1.1. Most of the methodology for measuring the characteristics of antennas was developed before and during World War II. The basic methods for the measurement of antenna far field patterns, antenna polarization, antenna input impedance, gain and directivity were developed during the above period in conjunction with the design of novel radiating structures, which were needed in the rapidly expanding telecommunication and radar technology.

1.2. However, it was soon understood that antenna metrology requires not only sound theoretical background to develop efficient measurement techniques but also sophisticated (and very expensive) equipment capable of providing the necessary accuracy and purity of the measured data. Commercial equipment specifically designed for antenna measurements was introduced much later (in the 1960s) due, in part, to the requirements of aerospace, space and defence industry.

1.3. The equipment specifically designed for antenna measurements includes: antenna ranges, antenna positioners, pattern recorders, signal generators, antenna gain standards, etc. Later on, sophisticated computer systems were developed to provide automated control of pattern measurements, and fast calculations related to antenna directivity, 2-D to 3-D pattern conversion, near-to-far field transformations (in compact antenna ranges), etc.

2. General requirements for antenna measurement procedures

2.1. The ideal condition for measuring the far-field characteristics of an antenna is its illumination by a *uniform plane wave*. This is a wave, which has a plane wave front with the field vectors being constant across it. For example, the electric field vector $\vec{E}$ of a uniform (non-attenuating) plane wave propagating in the $+z$ -direction is described by the general 1-D wave expression:

$$\vec{E}(z,t) = \hat{u}_e \; E_m \; f(t - z/v) \tag{1}$$

Here, $\hat{u}_e(z,t)$ describes the polarization of the $\vec{E}$ -vector, and, generally, it may depend on time and position. Notice that the $\vec{E}$ -vector does not depend on the x and y coordinates, i.e. its magnitude E_m is constant across any $x-y$ plane. The field vectors depend only on the z coordinate through the argument of the waveform $f(t - z/v)$.

2.2. In practice, antennas in 3-D space generate far fields, which are closely approximated by spherical wave fronts when the observation point is sufficiently far away from the source. However, at large distances from the source antenna, the curvature of the phase front is small over the aperture of the test antenna, and it is well approximated by a uniform plane wave.

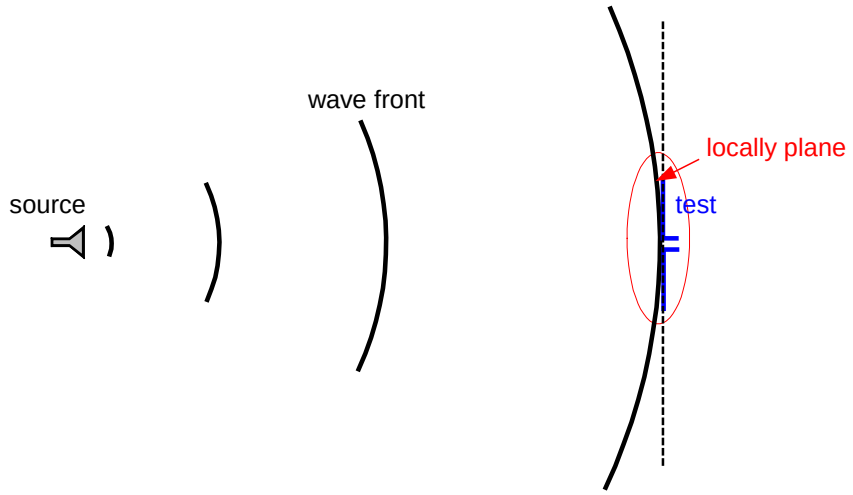

2.3. It was already shown in LO6 (6.1.6) that if the distance from the source is equal to the inner boundary of the far field region of that source, $R_{\min}^{far} = 2D_{\max}^2 / \lambda$, then the maximum phase error of the incident field from the ideal plane wave is about $e_{\max} \simeq 22.5^\circ = \pi/8$ rad. Here, $D_{\max}$ is the maximum dimension of the source antenna.

2.4. We will now show that if $D_{\max}$ is the maximum dimension of the antenna under test (AUT), a distance $R_{\min}$ from the source of a spherical wave given by

$$R_{\min} = 2D_{\max}^2 / \lambda \tag{2}$$

will ensure that the maximum phase difference between a plane wave and the spherical wave at the aperture of the AUT is $e_{\max} \simeq 22.5^\circ = \pi/8$ rad.

2.5. Consider a source of a spherical wave and an AUT located at a distance R away from it.

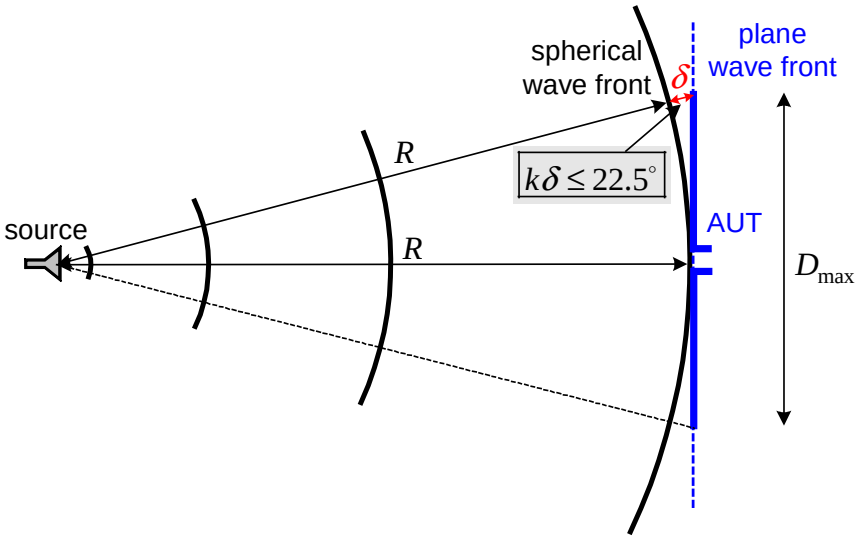

The largest phase difference between the spherical wave and the plane wave appears at the edges of the AUT, which corresponds to the difference in the wave paths, δ. This phase difference must fulfil the requirement:

$$k\delta \le \pi/8 \tag{3}$$

2.6. The difference in the wave paths, δ, is determined by noticing that

$$(R+\delta)^2 = R^2 + (D_{\max}/2)^2 \tag{4}$$

The only physical solution of the above quadratic equation for δ is:

$$\delta = \sqrt{R^2 + (D_{\max}/2)^2} - R \tag{5}$$

The above is approximated by the use of the binomial expansion (the first two terms only) as:

$$\delta = R\left[\sqrt{1+\left(\frac{D_{\max}}{2R}\right)^2} - 1\right] \simeq R\left[1+\frac{1}{2}\left(\frac{D_{\max}}{2R}\right)^2 - 1\right] = \frac{D_{\max}^2}{4R} \tag{6}$$

2.7. The minimum distance from the source of the spherical wave is now determined from the requirement in (3).

$$k\frac{D_{\max}^2}{4R} = \frac{2\pi}{\lambda}\frac{D_{\max}^2}{4R} \le \frac{\pi}{8} \tag{7}$$

Thus,

$$\boxed{R_{\min} = 2D_{\max}^2/\lambda} \tag{8}$$

2.8. The requirement for a very small wave front curvature leads to a major difficulty in antenna measurements: large separation distances are required between the source antenna and the AUT. Thus, the larger the AUT, the larger measurement site is required. While the size of the site may not be a problem, securing its reflection-free, noise-free, and EM interference-free environment is extremely difficult.

2.9. Special attention must be paid to minimizing unwanted reflections from nearby objects (equipment, personnel, buildings), from the ground or the walls of the site. This makes the open sites for antenna measurements (open ranges) a very rare commodity since they have to provide free-space propagation. Such ideal conditions are found only in unpopulated (desert) areas of predominantly flat terrain. The other alternative is offered by indoor chambers, which minimize reflections by special wall lining with RF/microwave absorbing material. They are very much preferred to open ranges because of their clean and controlled environment. Unfortunately, they are very expensive and often they cannot accommodate large antennas.

2.10. There are cases in which the antenna operates in a very specific environment (mounted on an aircraft, mobile system, etc.). In such cases, it is better to measure the antenna as it is mounted, i.e., in its own environment. Such measurements are very specific and often cannot be performed in indoor chambers (anechoic chambers).

2.11. Here is a summary of the drawbacks associated with experimental antenna investigations (antenna measurements).

- They are affected by unwanted reflections.
- Often, they require too large separation distances.
- They are very complicated when a whole antenna system (on-craft mounted antenna) is to be measured.
- Outdoor measuring sites provide uncontrollable EM environment, which besides all depends on the weather.
- Indoor measuring sites cannot accommodate large antenna systems.
- Antenna measurement technology is very expensive.

3. Antenna ranges (AR)

3.1. The facilities for antenna measurements are called *antenna ranges* (AR). They can be categorized as outdoor ranges and indoor ranges (anechoic chambers). According to the principle of measurement, they can be also categorized as: reflection ranges, free-space ranges, and compact ranges.

3.2. The reflection ranges are designed so that the reflection (usually from ground) is used to create constructive interference and a uniform wave front in the region of the AUT. Such a region is called the “quite zone”. Reflection ranges are usually of the outdoor type. They are used to measure antennas of moderately broad patterns operating in the UHF frequency bands (500-1000 MHz).

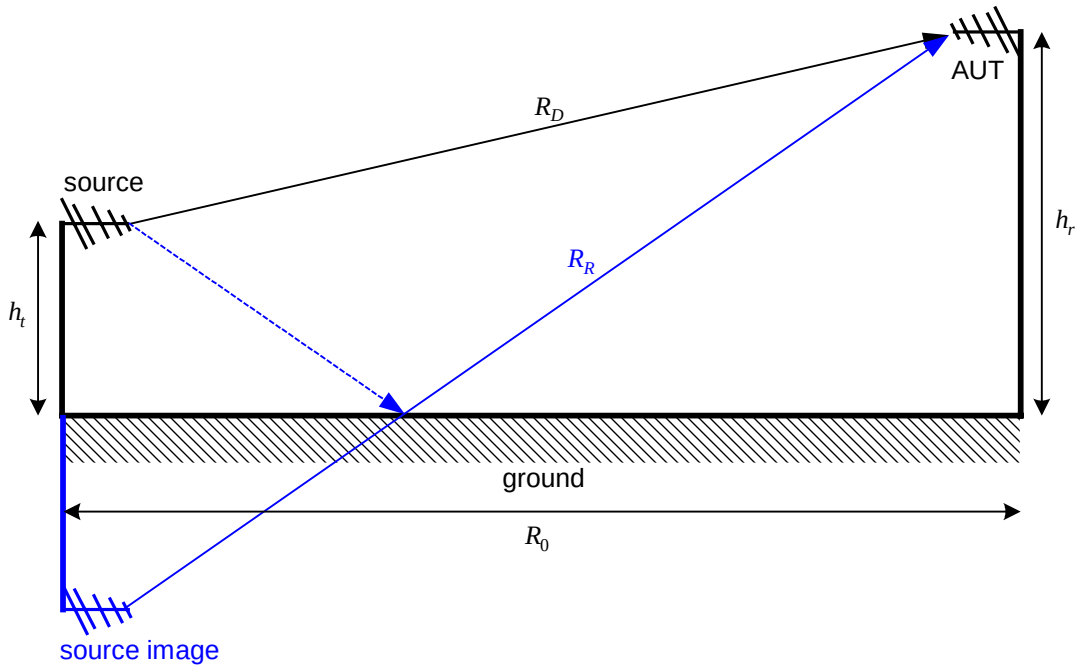

3.3. The design of reflection ranges is rather complicated and depends on the reflection coefficient of the ground (the range's surface), its smoothness, as well as the pattern of the source antenna. The main parameter to be determined is the height of the mast, on which the AUT is to be mounted h_r, provided that the height of the transmitting antenna h_t is known. Detailed information is provided in

L.H. Hemming and R.A. Heaton, "Antenna gain calibration on a ground reflection range," *IEEE Trans. on Antennas and Propagation*, vol. AP-21, pp. 532-537, July 1977.

3.4. The free-space ranges provide reflection-free propagation of the EM waves. They can be outdoor or indoor. ***Outdoor free-space ranges*** are carefully built in such a way that reflections from buildings and other objects are minimized. Outdoor free-space ranges can be realized as *elevated ranges* and *slant ranges*. ***Indoor ranges*** suppress reflections (echoes) by lining the walls, the floor and the ceiling with special RF/microwave absorbers. The indoor free-space ranges are called *anechoic chambers*.

3.5. The elevated ranges are characterized by the following features:

- Both antennas (the transmitting and the receiving) are mounted on high towers or buildings.
- The terrain beneath is smooth.
- The source antenna has very low side lobes so that practically there is no energy directed toward the surface below (the ground) or the buildings behind.
- The line-of-sight is always clear.

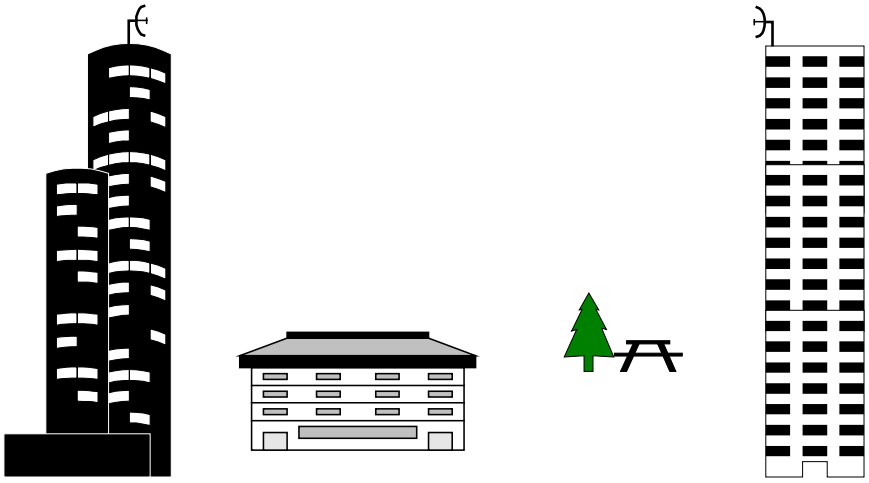

3.6. The slant ranges use up less space than the elevated ranges. The test antenna is mounted at a fixed height on a non-conducting tower (e.g. made of fiber glass), while the source antenna is mounted near the ground. The source antenna must have its pattern null pointed toward ground. It is desirable that it has very low side lobes, too. Slant ranges still require wide open space to minimize reflections from surrounding buildings.

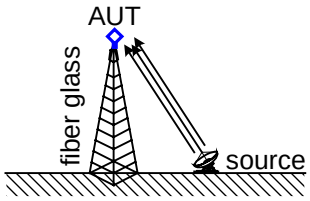

3.7. The anechoic chambers are the most popular antenna measurement sites especially in the microwave frequency range. They provide convenience and controlled EM environment. However, they are very expensive and complex facilities. An anechoic chamber is typically a large room whose walls, floor and ceiling are first EM isolated by steel sheets. In effect, it is a huge Faraday cage, which provides ideal security against outer EM noise and interference. Besides, all inner surfaces of the chamber are lined with RF/microwave absorbers. An anechoic chamber is shown in the figure below.

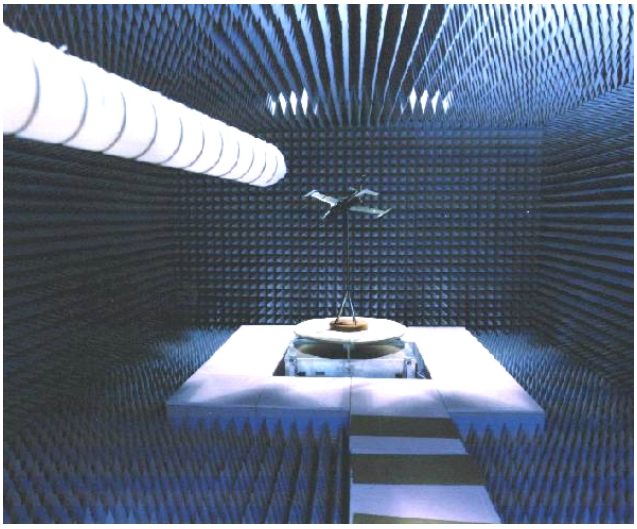

3.8. The first EM wave absorbers were developed during World War II in both US and German laboratories. The manufacturing of anechoic chambers became possible after RF/microwave absorbing materials with improved characteristics had become commercially available. The first broad band absorbers were made of a material called hairflex. Hairflex was made of animal fibres sprayed with (or dipped in) conducting carbon in neoprene. A historical summary of the development of EM wave absorbing materials is given by Emerson in his paper:

W.H. Emerson, "Electromagnetic wave absorbers and anechoic chambers through the years," *IEEE Trans. on Antennas and Propagation*, vol. AP-21, pp. 484-489, July 1973.

3.9. Nowadays, absorbing elements are with much improved characteristics providing reflection coefficients as low as –50 dB at normal incidence for a thickness of about four wavelengths. Reflection increases as the angle of incidence increases. For example, a typical reflection of –25 dB is related to an angle of incidence of about 70 degrees.

3.10. A typical absorbing element has the form of a pyramid or a wedge. Pyramids are designed to absorb best the waves at normal (nose-on) incidence, while they do not perform very well at large angles of incidence. They act, in effect, as a tapered impedance transition for normal incidence of the EM wave from the intrinsic impedance of 377 Ω to the short of the chamber's wall. Their resistance gradually decreases as the pyramid's cross-section increases.

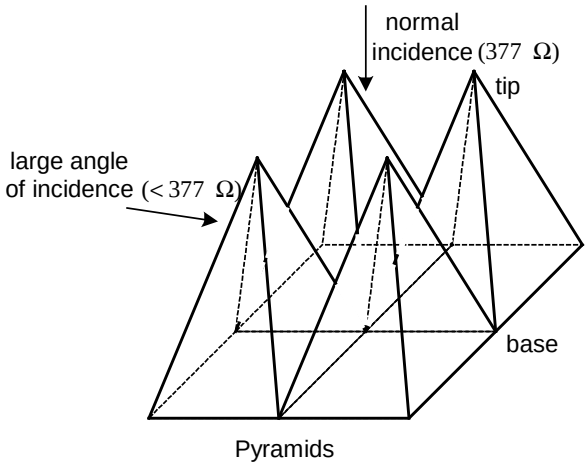

Pyramids

3.11. Wedges, on the other hand, perform much better than pyramids for waves, which travel nearly parallel to their ridges.

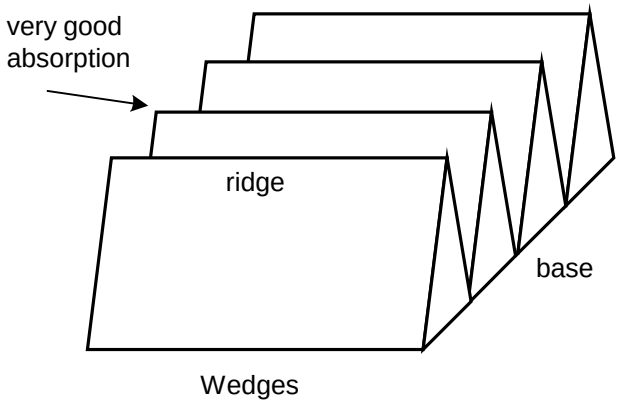

Wedges

For more detailed information on absorbing materials and shapes see:

John Kraus, *Antennas*, 2nd edition, McGraw-Hill, Inc.

B.T. DeWitt and W.D. Burnside, "Electromagnetic scattering by pyramidal and wedge absorber," *IEEE Trans. on Antennas and Propagation*, 1988.

An anechoic chamber lined with both types of absorbing shapes is shown below.

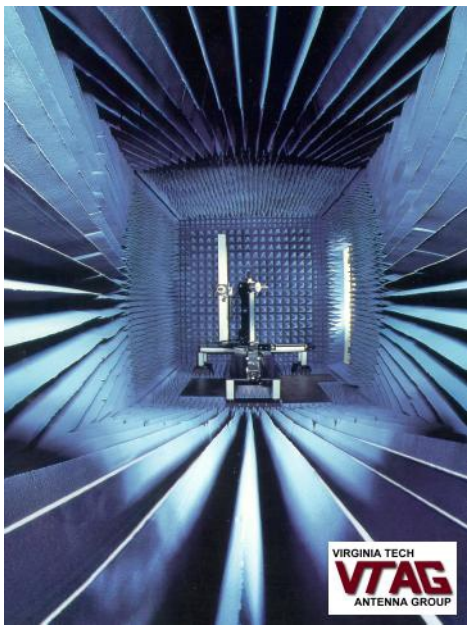

3.12. There are two types of anechoic chamber designs: rectangular chambers and tapered chambers. The design of both chamber types is based on geometrical optics considerations, whose goal is to minimize the amplitude and phase ripples in the test zone (the quiet zone), which are due to the imperfect absorption by the wall lining. The tapered chamber has the advantage of tuning by moving the source antenna closer to (at higher frequencies) or further from (at lower frequencies) the apex of the taper. Thus, the reflected rays are adjusted to produce nearly constructive interference with the direct rays at the test location.

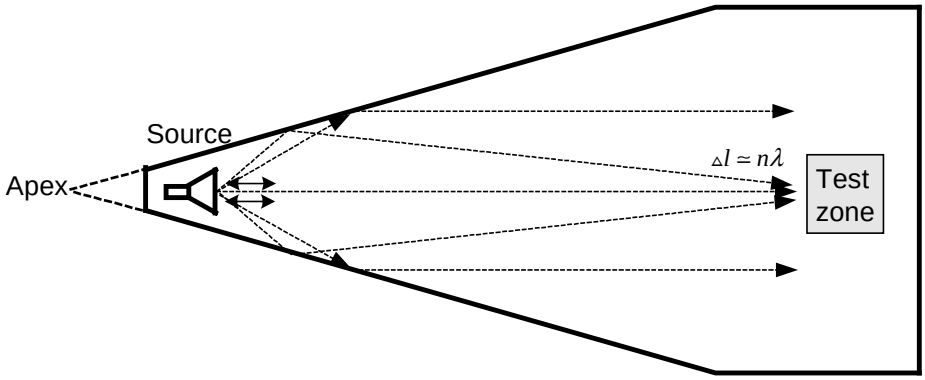

3.13. Simple anechoic chambers are limited by the distance requirements of the far-field measurements of large antennas or scatterers. There are two basic approaches to overcome this limitation. One is presented by the Compact Antenna Test Ranges (CATRs), which produce a nearly uniform plane wave in a very short distance via a system of reflectors (or a single paraboloidal reflector). Another approach is presented by techniques based on near-to-far field transformation, where the measurements are performed in the near-field zone or in the Frennel zone of the AUT.

3.14. The Compact Antenna Test Range (CATR) utilizes a precision paraboloidal antenna to collimate the energy of a primary feed antenna in a short distance (about 10 to 20 m). Typical arrangement of a compact range is as shown below.

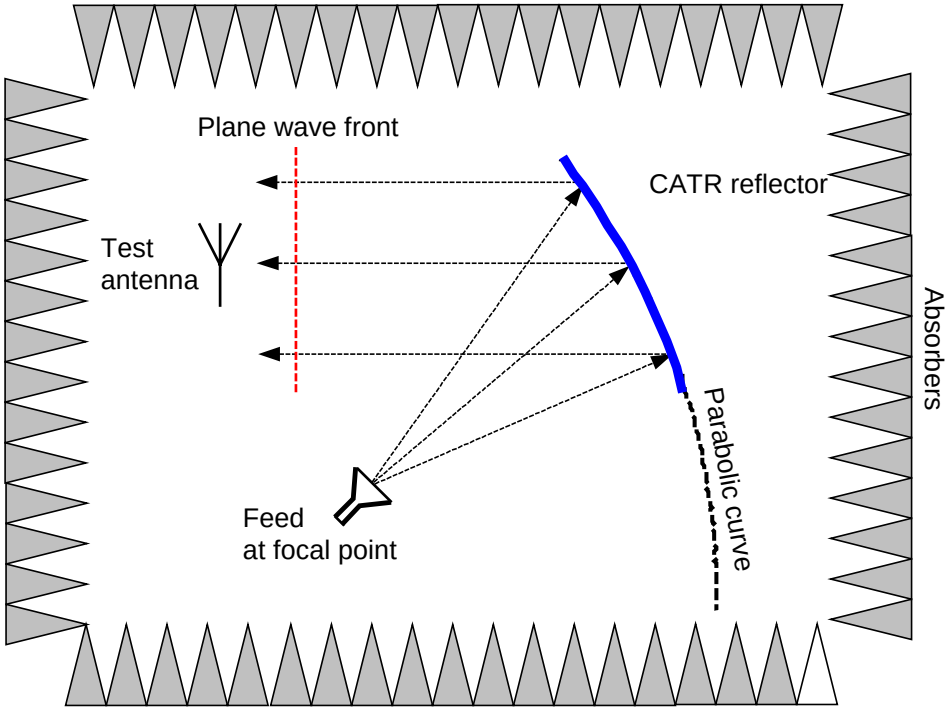

3.15. The linear dimensions of the reflector must be at least three to four times those of the test antenna in order the illumination of the test antenna to sufficiently approximate a uniform plane wave. An offset feed is used for the reflector to prevent aperture blockage and to reduce the diffraction from the primary feed structure. The paraboloidal reflector surface must be fabricated with very high precision to obtain fairly uniform amplitude distribution of the incident field at the test antenna.

3.16. A perfect plane wave is produced by the CATR if the paraboloidal reflector has a perfect surface, infinite size, and if the feed is a point source with a pattern to ideally compensate for the space attenuation. Of course, such ideal conditions cannot be achieved, and the field distribution in a real

CATR deviates from the uniform plane wave. However, it is within acceptable parameters in the so called “quite zone”, which is also the test zone, where the AUT is positioned.

3.17. The quiet zone is typically 50-60% the size of the reflector. The imperfections of the field in the quiet zone are measured in terms of phase errors, ripple amplitude deviations, and taper amplitude deviations. Acceptable deviations for most CATRs are: less than 10% phase error, less than 1dB ripple and taper amplitude deviations.

3.18. Amplitude taper in the quiet zone is attributed to two sources: the primary feed pattern and the space attenuation. The primary feed is not isotropic; therefore, its pattern has certain variation with direction. Usually, the pattern gradually decreases as the directional angles point away from the antenna’s axis. This is called the feed amplitude taper. That portion of the feed pattern, which illuminates the CATR surface, is directly transferred into the quiet zone, thus contributing to the field amplitude taper deviation from the ideal uniform plane wave.

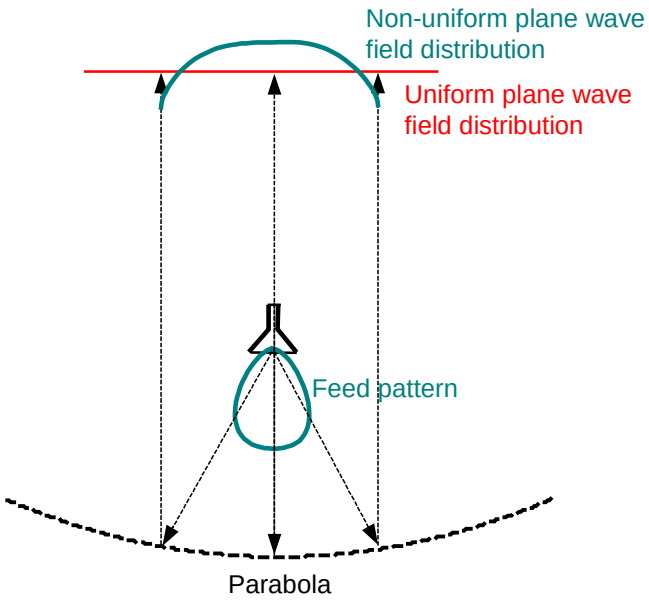

3.19. It is obvious that if the feed pattern is nearly isotropic for the angles illuminating the reflector, the feed amplitude taper will be very small. That is why low-directivity antennas are preferred as feeds. However, the feed cannot be omnidirectional because direct illumination of the AUT by the primary feed is unacceptable. The careful choice of the feed antenna and its location is of paramount importance for the CATR design.

3.20. The $1/r^2$ space attenuation occurs with the spherical spreading of the uncollimated energy radiated by the primary feed towards the reflector. The paths of these primary EM rays from the feed to the reflector are of different lengths, which results in different amplitude across the front of the reflected collimated EM wave. This is yet another reason for amplitude taper deviations in the quiet zone.

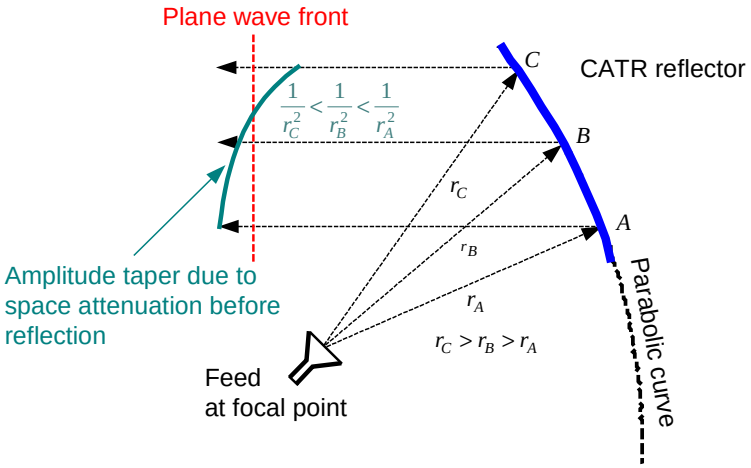

3.21. Amplitude and phase ripples in the quiet zone are primarily caused by diffraction from the edges of the reflector. The diffracted field is spread in all directions interfering with the major reflected field in constructive and destructive patterns. The result is the appearance of maxima and minima of the field amplitude across the plane wave front in the quiet zone. Diffraction from edges causes deviation of the phase of the plane wave, too.

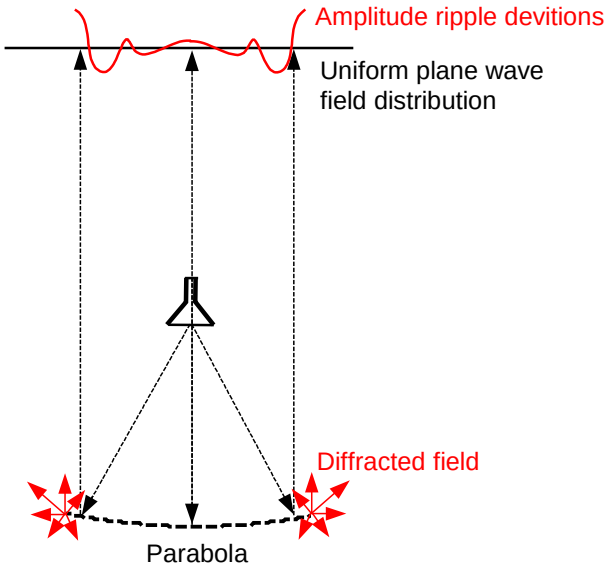

3.22. There are two popular ways to reduce diffraction from reflector edges: serrated-edge reflectors and rolled-edge reflectors. Rolled-edge modifications at the edge of the reflector are introduced to direct the diffracted field mainly to the side and the back of the reflector.

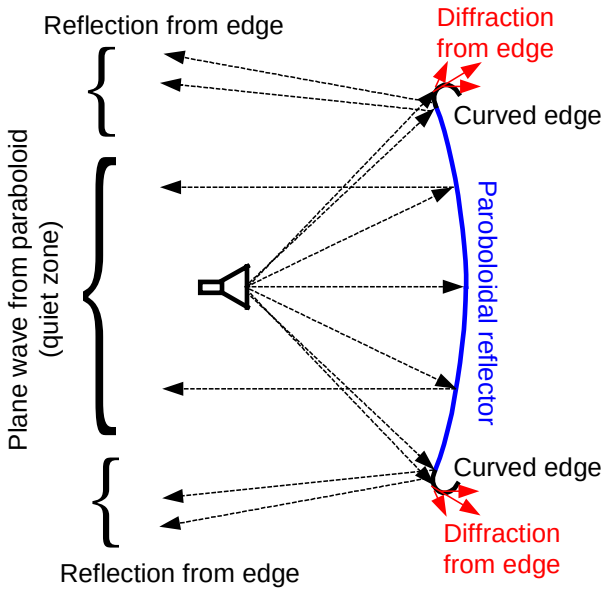

3.23. Serrated edges of reflectors produce multiple low-amplitude diffractions, which are randomized in amplitude, phase and polarization. That is why the probability of their cancellation in any point of the quiet zone is high. Serrations are typically of irregular triangular shape. To further reduce the diffraction in the direction of the test zone, the serrated edges may be also rolled backwards. A photograph of a compact range whose reflector has serrated edges is shown below.

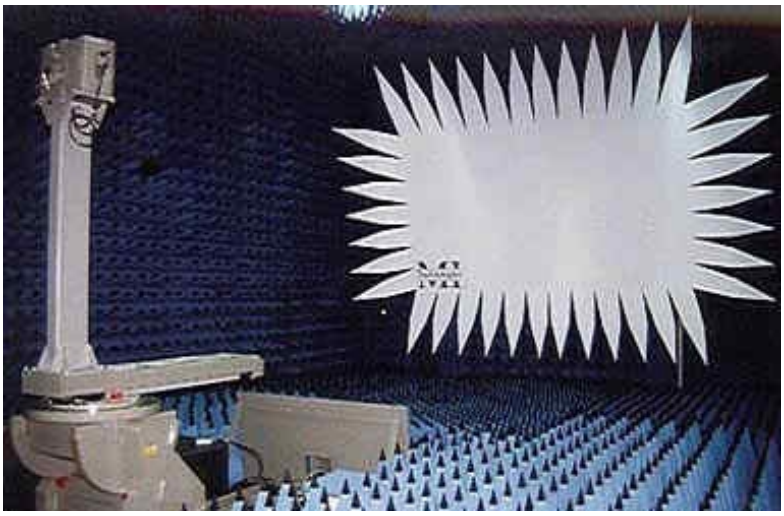

3.24. Another modern approach for measuring far-field patterns, which allows for the most compact chambers, is the near-field/far-field (NF/FF) method. The field amplitude, phase and polarization are measured in the near field of the AUT, which is in radiating mode. The near-field data is transformed to far-field patterns via analytical techniques implemented in the sophisticated software run by an automated computer system, which controls the measurement procedure.

3.25. The magnitude and phase of the tangential electric field are measured at regular intervals over a well-defined surface: a plane, a cylinder, or a sphere, located close to the AUT. The sampled E-field data is used to calculate the angular spectrum of plane, cylindrical or spherical waves, which matches closely the radiated field angular distribution. This is called ***modal expansion*** of the radiated field.

3.26. In principle, the measurement can be done over a surface, which can be defined in any of the six orthogonal-vector coordinate systems: rectangular, cylindrical (circular-cylindrical), spherical,

elliptic-cylindrical, parabolic-cylindrical, and conical. However, only the first three are deemed convenient for data acquisition, and of them, of course, the simplest one from technological point of view is the planar surface. The field is measured at the nodes of the mesh of the respective surface (see the figure below).

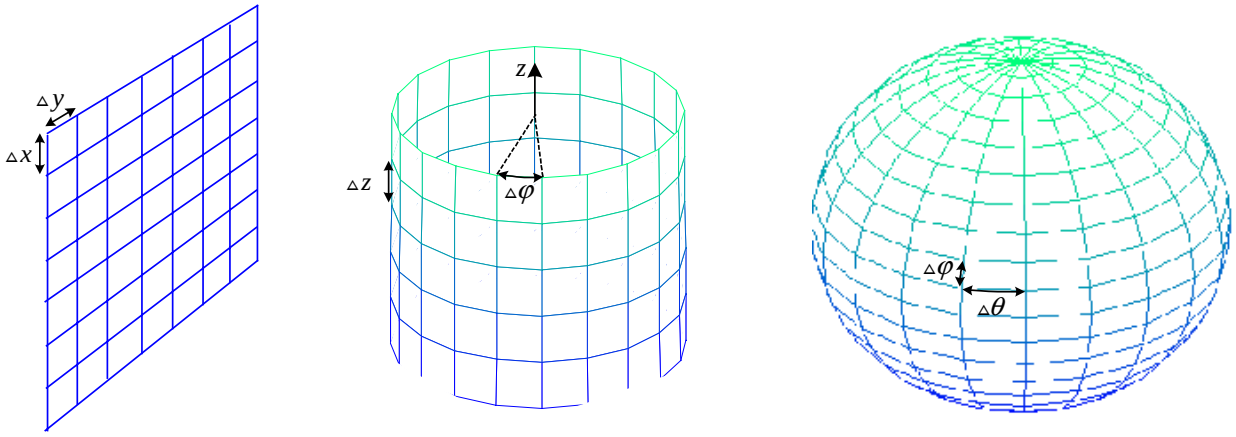

3.27. Here, we will consider the simplest data acquisition over a planar surface and its modal expansion. At this point, we will not discuss in detail Fourier transforms in antenna theory. It should suffice to state that ***the far-field radiation pattern of any aperture (surface) is the Fourier transform of the aperture field distribution***. We will now show the formulas associated with this statement in the simplest case of a planar aperture.

3.28. Assume that in the near-field measurements, the E-vector is being measured over a planar surface, which is our aperture. According to the ***equivalence principle***, we can now assume that the field behind the surface (on the side of the antenna) is equal to zero, and its impact on the field on the other side of the surface is due to equivalent surface currents defined at the surface as:

$$\vec{J}_s = \hat{n} \times \vec{H}_a$$
$$\vec{M}_s = -\hat{n} \times \vec{E}_a \qquad (9)$$

Here, $\vec{E}_a$ and $\vec{H}_a$ represent the field vectors at the aperture (the surface) created by the antenna behind it. $\vec{J}_s$ is the equivalent electric current density, $\vec{M}_s$ is the equivalent magnetic current density, and $\hat{n}$ is the surface unit normal pointing toward the region of observation (away from the antenna).

3.28. Since the field behind the plane surface is now set to zero, we can as well assume that the medium behind the surface is a perfect conductor. In the case of a flat surface, whose size is much larger than a wavelength, the image theory can be applied. Now, the equivalent surface sources become:

$$\vec{J}_s = 0; \;\; \vec{M}_s = -\hat{n} \times (2\vec{E}_a) \qquad (10)$$

3.29. The equivalent surface magnetic currents $\vec{M}_s$ create an electric vector potential $\vec{F}$, which, in the far zone, is calculated as:

$$\vec{F}(P) \simeq -\varepsilon \frac{e^{-jkr}}{4\pi r} \hat{n} \times \iint_{S_a} 2\vec{E}_a(\vec{r}\,') e^{j\vec{k}\cdot\vec{r}\,'} ds' = -\varepsilon \frac{e^{-jkr}}{2\pi r} \hat{n} \times \iint_{S_a} \vec{E}_a(\vec{r}\,') e^{j\vec{k}\cdot\vec{r}\,'} ds' \qquad (11)$$

Here, $\vec{r}\,' = \hat{x}\, x' + \hat{y}\, y'$ is the position vector of the integration point, and r is the distance from the observation point P to the origin.

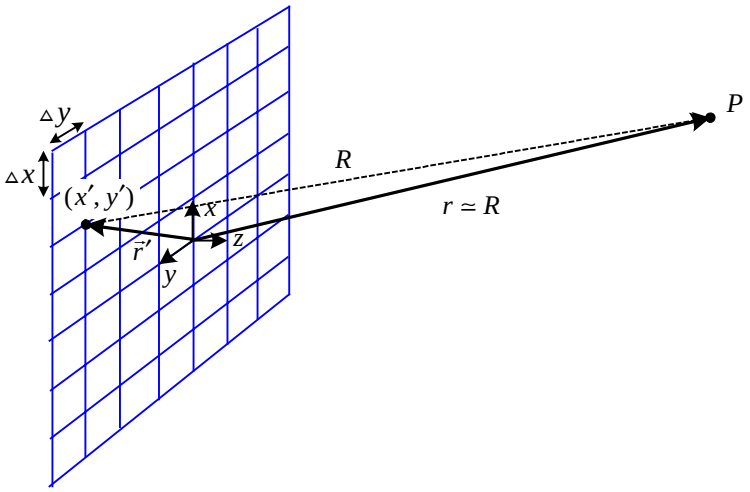

3.30. Note that the far-field approximations have been applied (see module LO6) to the amplitude and the phase term of the vector potential integral. The propagation vector $\vec{k} = k\hat{r}$ shows the direction of propagation, and has a magnitude equal to the wave number $k = \omega\sqrt{\mu\varepsilon}$. The scalar product $\vec{k} \cdot \vec{r}'$ yields the familiar phase term $\vec{k} \cdot \vec{r}' = kr' \cos\theta$, which in the case of z-oriented wire antennas becomes $\vec{k} \cdot \vec{r}' = kz' \cos\theta$ (see LO6).

3.31. We now remember that the far-field E-vector is related to the far-field electric vector potential as (see Module 3, equation (3.60)):

$$\vec{E}^{far} = -j\omega\eta\vec{F} \times \hat{r} \tag{12}$$

Here, $\eta = \sqrt{\mu/\varepsilon}$ is the intrinsic impedance of the medium of propagation. Substituting (11) in (12) yields:

$$\vec{E}^{far} \simeq -jk\frac{e^{-jkr}}{2\pi r}\hat{r} \times \iint_{S_a} (\hat{n} \times \vec{E}_a) e^{jk\vec{r}\cdot\vec{r}'} dx'dy' \tag{13}$$

3.32. In the case of a planar surface, its unit normal is constant, and we can assume that $\hat{n} \equiv \hat{z}$. Having in mind that the radial unit vector in rectangular coordinates is:

$$\hat{r} = \hat{x}\sin\theta\cos\varphi + \hat{y}\sin\theta\sin\varphi + \hat{z}\cos\theta\,, \tag{14}$$

one can calculate the x and y components of $\vec{E}^{far}$ as:

$$\boxed{E_x^{far} \simeq jk\frac{e^{-jkr}}{2\pi r} \cdot \cos\theta \cdot \iint_{S_a} E_{xa}(x', y') e^{j(k_x x' + k_y y')} dx'dy'} \tag{15}$$

$$\boxed{E_y^{far} \simeq jk\frac{e^{-jkr}}{2\pi r} \cdot \cos\theta \cdot \iint_{S_a} E_{ya}(x', y') e^{j(k_x x' + k_y y')} dx'dy'} \tag{16}$$

3.33. The z-component of the far E-field is found as:

$$E_z^{far} \simeq -jk\frac{e^{-jkr}}{2\pi r} \cdot \sin\theta \cdot \left[\cos\varphi \iint_{S_a} E_{xa}(x', y') e^{j(k_x x' + k_y y')} dx'dy' + \sin\varphi \iint_{S_a} E_{ya}(x', y') e^{j(k_x x' + k_y y')} dx'dy' \right] \tag{17}$$

It is obvious from (15), (16) and (17) that if the components E_x^{far} and E_y^{far} are known, the E_z^{far} component can be calculated from them as:

$$\boxed{E_z^{far} = -\tan\theta \left[E_x^{far}\cos\varphi + E_y^{far}\sin\varphi \right]} \tag{18}$$

3.34. Let us pay more attention to the integrals appearing in equations (15) and (16):

$$f_x(k_x, k_y) = \iint_{S_a} E_{xa}(x', y') e^{j(k_x x' + k_y y')} dx'dy' \tag{19}$$

$$f_y(k_x,k_y)=\iint_{S_a} E_{ya}(x',y')e^{j(k_x x'+k_y y')}dx'dy' \tag{20}$$

These integrals are nothing else but the double Fourier transforms of the field components' distribution over the area of the surface S_a, where the tangential E-field components are being measured. The surface is assumed infinite ($-\infty < x' < +\infty$, $-\infty < y' < +\infty$) although the field components may have zero values outside a given aperture.

3.35. The functions f_x and f_y depend on the spectral variables k_x and k_y, which are the components of the propagation vector $\vec{k}=k\hat{r}$ in the x - y plane:

$$\begin{aligned} k_x &= k\sin\theta\cos\varphi \\ k_y &= k\sin\theta\sin\varphi \end{aligned} \tag{21}$$

where $k=\omega\sqrt{\mu\varepsilon}=2\pi/\lambda$ is the wave number of the medium.

3.36. Note that the functions $f_x(k_x,k_y)$ and $f_y(k_x,k_y)$ give the far-field pattern in terms of x and y components for small θ when $\cos\theta\approx 1$ because they become almost identical with the normalized far-field E-components.

$$\left.\begin{aligned} \bar{E}_x^{far} &\approx f_x(k_x,k_y) \\ \bar{E}_y^{far} &\approx f_y(k_x,k_y) \end{aligned}\right\},\ \cos\theta\simeq 1 \tag{22}$$

This finally clarifies the statement made in 3.27.

3.37. The far-field z -component can be also expressed by its spectral counterpart $f_z(k_x,k_y)$ in the same manner as the x and y components:

$$E_z^{far} = jk\frac{e^{-jkr}}{r}\cdot\cos\theta\cdot f_z(k_x,k_y) \tag{23}$$

Having in mind (17) and (18), it becomes clear that $f_z(k_x,k_y)$ is not an independent function but is related to the other two spectral components as:

$$\boxed{f_z(k_x,k_y)=-\tan\theta\left[\,f_x(k_x,k_y)\cos\varphi+f_y(k_x,k_y)\sin\varphi\,\right]} \tag{24}$$

3.38. We can now define the vector plane wave spectral function:

$$\vec{f}(k_x,k_y)=\hat{x}f_x(k_x,k_y)+\hat{y}f_y(k_x,k_y)+\hat{z}f_z(k_x,k_y) \tag{25}$$

whose spatial components are calculated via (19), (20) and (24). The far-field E-vector can be calculated from the spectral function as:

$$\boxed{\vec{E}(r,\theta,\varphi)\simeq jk\frac{e^{-jkr}}{2\pi r}\cos\theta\cdot\vec{f}(k_x,k_y)} \tag{26}$$

3.39. One can express the vector equation (26) in terms of the θ and φ components of the far-field E-vector:

$$\begin{aligned} E_\theta(r,\theta,\varphi) &\simeq jk\frac{e^{-jkr}}{2\pi r}\cos\theta\cdot f_\theta(k_x,k_y) \\ E_\varphi(r,\theta,\varphi) &\simeq jk\frac{e^{-jkr}}{2\pi r}\cos\theta\cdot f_\varphi(k_x,k_y) \end{aligned} \tag{27}$$

Since the spectral function $\vec{f}$ is derived via its rectangular components during the data acquisition over a planar surface, it is desirable to convert f_θ and f_φ to f_x and f_y.

3.40. Following the standard transformation from spherical to rectangular components, one obtains:

$$f_\theta\ \cos\theta=\cos\theta\left(f_x\cos\theta\cos\varphi+f_y\cos\theta\sin\varphi-f_z\sin\theta\right) \tag{28}$$

After substituting f_z with its equivalent expression (24), one arrives at:

$$f_\theta\cos\theta=f_x\cos\varphi+f_y\sin\varphi \tag{29}$$

In analogous manner, it can be shown that

$$f_\varphi\cos\theta=-f_x\sin\varphi+f_y\cos\varphi \tag{30}$$

3.41. The substitution of (29) and (30) into (27) finally yields:

$$E_\theta(r,\theta,\varphi) \simeq jk\frac{e^{-jkr}}{2\pi r}(f_x\cos\varphi + f_y\sin\varphi)$$
$$E_\varphi(r,\theta,\varphi) \simeq jk\frac{e^{-jkr}}{2\pi r}(-f_x\sin\varphi + f_y\cos\varphi) \quad (31)$$

3.42. We can now summarize the procedure of the NF/FF pattern measurement in three basic steps:

- Measure the tangential E-field components $E_{ax}(x',y',z'=0)$ and $E_{ay}(x',y',z'=0)$ over the near-field aperture (data acquisition).
- Calculate the plane wave spectral functions $f_x(k_x,k_y)$ and $f_y(k_x,k_y)$ using (19) and (20).
- Calculate the normalized far-field components using

$$\bar{E}_\theta(\theta,\varphi) \simeq f_x\cos\varphi + f_y\sin\varphi$$
$$\bar{E}_\varphi(\theta,\varphi) \simeq -f_x\sin\varphi + f_y\cos\varphi \quad , \quad (32)$$

  or, the total normalized field patterns using

$$\bar{E}(\theta,\varphi) = \sqrt{\bar{E}_\theta^2(\theta,\varphi) + \bar{E}_\varphi^2(\theta,\varphi)} = \sqrt{f_x^2(k_x,k_y) + f_y^2(k_x,k_y)} \quad (33)$$

3.43. In the actual experimental procedure, a planar surface is chosen a distance z_0 away from the test antenna, which is in radiating mode. We will call this surface the measurement aperture. The distance z_0 must be at least three wavelengths away from the antenna, so that the measurement is carried out in the radiating near field region (Frennel zone) rather than in the reactive near-field region.

3.44. The measurement aperture is rectangular of dimensions $a\times b$. The measurement aperture is divided into M×N points spaced evenly $\triangle x$ and $\triangle y$ apart. The relation between the number of points and the respective spacing is then:

$$M = \frac{a}{\triangle x} + 1$$
$$N = \frac{b}{\triangle y} + 1 \quad (34)$$

3.45. Thus, the sampling points are located at coordinates $(m\triangle x, n\triangle y, 0)$, where $0 \le m \le M-1$ and $0 \le n \le N-1$. The separation distances $\triangle x$ and $\triangle y$ must be less than half a wavelength in order to satisfy Nyquist's sampling criterion, and such that the equations in (34) yield integer numbers. The measurement aperture must be large enough so that the signal at its edges is at least 45 dB down from the maximum measured signal over the entire surface.

3.46. The plane wave spectral function $\vec{f}(k_x,k_y)$ can be evaluated at a discrete set of wave numbers as dictated by the discrete Fourier transform:

$$k_x = m\frac{2\pi}{a} = m\frac{2\pi}{(M-1)\triangle x}$$
$$k_y = n\frac{2\pi}{b} = n\frac{2\pi}{(N-1)\triangle x} \quad (35)$$

Conventional two-dimensional FFT (Fast Fourier Transform) techniques are used to perform this transformation.

3.47. The acquisition of the planar near-field data is done by a computer-controlled probe antenna (typically a waveguide horn or an open waveguide), which is moved to each grid node over the measurement aperture by a high-precision positioning system (positioner). The probe's axis is held stationary and normal to the measurement aperture. The probe must be linearly polarized so that separate measurements of the two tangential field components E_x and E_y become possible.

3.48. As the probe location changes, its pattern orientation with respect to the AUT changes, too, as shown below. The probe's partial directivities in the direction of the test antenna must be taken into account using probe compensation techniques.

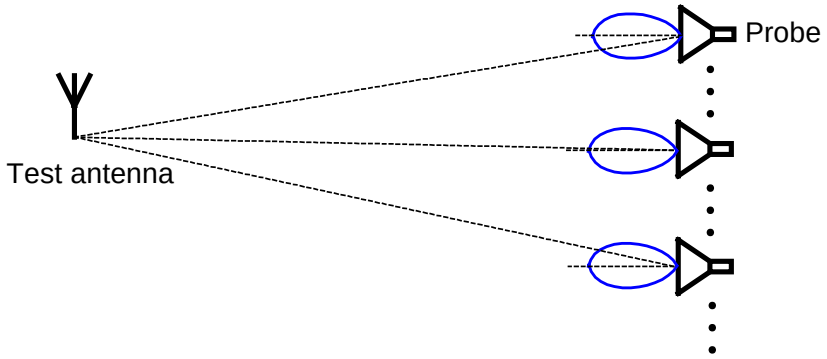

3.49. The principal advantage of the planar NF/FF transformation over the cylindrical and the spherical one is its mathematical simplicity. Its major disadvantage is that it cannot cover all directional angles. In the ideal case of infinite planar measurement surface, only one hemisphere of the antenna pattern can be measured. Thus, the back lobes and the side lobes of the antenna cannot be measured together with the main beam. Of course, the AUT can be rotated in different positions, so that the overall pattern can be constructed.

The reader interested in the subject of NF/FF transforms and measurements is referred to the following popular sources:

R.C. Johnson, H.A. Ecker, and J.S. Hollis, "Determination of far-field antenna patterns from near-field measurements," *Proc. IEEE*, vol. 61, No. 12, pp. 1668-1694, Dec. 1973.

D.T. Paris, W.M. Leach, Jr., and E.B. Joy, "Basic theory of probe compensated near-field measurements," *IEEE Trans. on Antennas and Propagation*, vol. AP-26, No. 3, pp. 373-379, May 1978.

E.B. Joy, W.M. Leach, Jr., G.P. Rodrigue, and D.T. Paris, "Applications of probe compensated near-field measurements," *IEEE Trans. on Antennas and Propagation*, vol. AP-26, No. 3, pp. 379-389, May 1978.

A.D. Yaghjian, "An overview of near-field antenna measurements," *IEEE Trans. on Antennas and Propagation*, vol. AP-34, pp. 30-45, January 1986.

4. Far-field pattern measurements

4.1. The far-field patterns are measured on the surface of a sphere of constant radius. Any position on the sphere is identified by the standard directional angles θ and φ of the spherical coordinate system. In general, the pattern of an antenna is 3-dimensional. However, 3-dimensional pattern acquisition is impractical, and a number of 2-D pattern measurements are performed. The minimal number of 2-dimensional patterns is two, and these two patterns must be in two orthogonal planes.

4.2. The pattern measurements are performed in 2-D pattern cuts. A simplified block diagram of a pattern measurement system is given below.

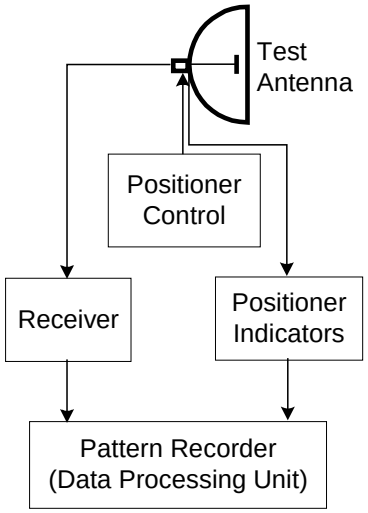

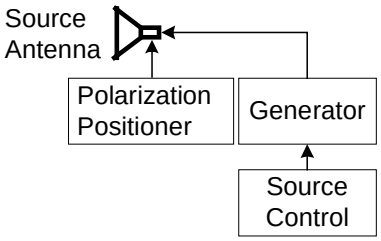

4.3. The total ***amplitude pattern*** is described by the vector sum of the two orthogonally polarized radiated field components, e.g.:

$$|\vec{E}| = \sqrt{|E_\theta|^2 + |E_\varphi|^2} \tag{36}$$

Rarely, the separate patterns for both components are needed. In this case, the polarization of the test antenna must be measured, too.

4.4. The entire 3-D pattern of the antenna can be approximated making use of the 2-D pattern acquisitions. Generally, for antennas of low directivity, at least three 2-D pattern cuts (in the three principal planes (e.g., $\varphi = 0^\circ$, $\varphi = 90^\circ$ and $\theta = 90^\circ$) are necessary in order to obtain good 3-D pattern approximation. For high-directivity antennas, only two orthogonal 2-D patterns will suffice. Assuming that the antenna axis is along the z-axis, these are the patterns at $\varphi = 0^\circ$ and $\varphi = 90^\circ$.

4.5. High-directivity antennas such as aperture antennas (horn antennas, reflector antennas), have their far field components expressed as:

$$E_\theta(\theta,\varphi) = jk\frac{e^{-jkr}}{4\pi r}[\mathcal{J}_x^E \cos\varphi + \mathcal{J}_y^E \sin\varphi + \eta\cos\theta(\mathcal{J}_y^H \cos\varphi - \mathcal{J}_x^H \sin\varphi)] \tag{37}$$

$$E_\varphi(\theta,\varphi) = jk\frac{e^{-jkr}}{4\pi r}[-\eta(\mathcal{J}_x^H \cos\varphi + \mathcal{J}_y^H \sin\varphi) + \cos\theta(\mathcal{J}_y^E \cos\varphi - \mathcal{J}_x^E \sin\varphi)] \tag{38}$$

Here, $\mathcal{J}_x^E$, $\mathcal{J}_y^E$, $\mathcal{J}_x^H$ and $\mathcal{J}_y^H$ are the familiar plane wave spectral functions:

$$\mathcal{J}_x^E(\theta,\varphi) = \iint_{S_A} E_{a_x}(x',y')e^{jk(x'\sin\theta\cos\varphi + y'\sin\theta\sin\varphi)}dx'dy' \tag{39}$$

$$\mathcal{J}_y^E(\theta,\varphi) = \iint_{S_A} E_{a_y}(x',y')e^{jk(x'\sin\theta\cos\varphi + y'\sin\theta\sin\varphi)}dx'dy' \tag{40}$$

$$\mathcal{J}_x^H(\theta,\varphi) = \iint_{S_A} H_{a_x}(x',y')e^{jk(x'\sin\theta\cos\varphi + y'\sin\theta\sin\varphi)}dx'dy' \tag{41}$$

$$\mathcal{J}_y^H(\theta,\varphi) = \iint_{S_A} H_{a_y}(x',y')e^{jk(x'\sin\theta\cos\varphi + y'\sin\theta\sin\varphi)}dx'dy' \tag{42}$$

4.6. From equations (37) and (38) it follows that the field components in the principal planes are:

$$E_\theta(\theta,\varphi = 0^\circ) = E_\theta(0) = jk\frac{e^{-jkr}}{4\pi r}[\mathcal{J}_x^E + \mathcal{J}_y^H \eta\cos\theta] \tag{43}$$

$$E_\theta(\theta,\varphi = 90^\circ) = E_\theta(90) = jk\frac{e^{-jkr}}{4\pi r}[\mathcal{J}_y^E - \mathcal{J}_x^H \eta\cos\theta] \tag{44}$$

$$E_\varphi(\theta,\varphi=0^\circ)=E_\varphi(0)=\ jk\frac{e^{-jkr}}{4\pi r}[-\eta\mathfrak{J}_x^H+\mathfrak{J}_y^E\cos\theta] \tag{45}$$

$$E_\varphi(\theta,\varphi=90^\circ)=E_\varphi(90)=\ jk\frac{e^{-jkr}}{4\pi r}[-\eta\mathfrak{J}_y^H-\mathfrak{J}_x^E\cos\theta] \tag{46}$$

4.7. It is, therefore, clear that the 3-D field dependence on the directional angles can be derived from the 2-D dependences in the equations (43) through (46) as:

$$\vec{E}(\theta,\varphi)=\ jk\frac{e^{-jkr}}{4\pi r}[\cos\varphi\ \vec{E}(\theta,\varphi=0^\circ)+\sin\varphi\ \vec{E}(\theta,\varphi=90^\circ)]\,, \tag{47}$$

where:

$$\vec{E}(\theta,\varphi=0^\circ)=\hat{\theta}\ E_\theta(0)+\hat{\varphi}\ E_\varphi(0)\,;$$

$$\vec{E}(\theta,\varphi=90^\circ)=\hat{\theta}\ E_\theta(90)+\hat{\varphi}\ E_\varphi(90)$$

4.8. The total 3-D amplitude pattern of the field defined in (47) is obtained as:

$$|\vec{E}(\theta,\varphi)|=\sqrt{\cos^2\varphi\ [\underbrace{E_\theta^2(0)+E_\varphi^2(0)}_{|\vec{E}(\theta,0^\circ)|^2}]+\sin^2\varphi\ [\underbrace{E_\theta^2(90)+E_\varphi^2(90)}_{|\vec{E}(\theta,90^\circ)|^2}]+\sin 2\varphi[E_\theta(0)E_\theta(90)+E_\varphi(0)E_\varphi(90)]} \tag{48}$$

In the pattern considerations, we will drop the factor $jk\frac{e^{-jkr}}{4\pi r}$.

It is easy to show that the last term in (48) is equal to:

$$E_\theta(0)E_\theta(90)+E_\varphi(0)E_\varphi(90)=(1-\cos^2\theta)(\mathfrak{J}_x^E\mathfrak{J}_y^E+\eta^2\mathfrak{J}_x^H\mathfrak{J}_y^H) \tag{49}$$

4.9. For high-directivity antennas, the angles θ, at which the antenna has significant pattern values, are small, and the term given in (49) can be neglected. Thus, the approximation of the 3-D pattern in terms of two orthogonal 2-D patterns reduces to the simple expression:

$$|\vec{E}(\theta,\varphi)|\simeq\sqrt{\cos^2\varphi\ |\vec{E}(\theta,0^\circ)|^2+\sin^2\varphi\ |\vec{E}(\theta,90^\circ)|^2} \tag{50}$$

4.10. Sometimes, the ***phase pattern*** of the far field is also measured. This requires special equipment, which includes phase measuring circuits.

5. Gain measurements

5.1. The gain measurements require essentially the same environment as the pattern measurements, although they are not so very much sensitive to reflections and EM interference. To measure the gain of antennas operating above 1 GHz, usually, free-space ranges are used. Between 0.1 GHz and 1 GHz, ground-reflection ranges are used.

5.2. Below 0.1 GHz, directive antennas are very large and the ground effects become increasingly pronounced. Usually the gain at these frequencies is measured directly in the environment of operation. Same holds for high-frequency antennas operating in a complicated environment (mounted on vehicles or aircrafts).

5.3. We will consider three gain-measurement techniques. The first two belong to the so-called *absolute-gain measurements*, and they are: the ***two-antenna method***, and the ***three-antenna method***. The third method is called the ***gain-transfer*** (or ***gain-comparison***) ***method***.

5.4. The ***two-antenna method*** is based on Friis transmission equation and it needs two identical samples of the tested antenna. One of the identical samples is the radiating antenna, and the other one is the receiving antenna. Assuming that the antennas are well matched in terms of impedance and polarization (mutual alignment must be sufficiently good), the Friis transmission equation is:

$$\frac{P_r}{P_t}=\left(\frac{\lambda}{4\pi R}\right)^2 G_tG_r,\ \text{ where } G_t=G_r=G \tag{51}$$

5.5. The formula for the calculation of the gain in dB obtained from (51) is:

$$\boxed{G_{\text{dB}}=\frac{1}{2}\left[20\log_{10}\left(\frac{4\pi R}{\lambda}\right)+10\log_{10}\left(\frac{P_r}{P_t}\right)\right]} \tag{52}$$

One needs to measure accurately the distance between the two antennas R, the received power P_r, the transmitted power P_t, and the frequency $f = c/\lambda$, which would allow the calculation of the wavelength λ.

5.6. The ***three-antenna method*** is used when only one sample of the test antenna is available. Then, any other two antennas can be used to perform three measurements, which allow the calculation of the gains of all three antennas. All three measurements are made at a fixed known distance between the radiating and the transmitting antennas, R.

5.7. It does not matter whether an antenna is in a transmitting or in a receiving mode. What matters is that the three measurements involve all three possible pairs of antennas: antenna #1 and antenna #2; antenna #1 and antenna #3; and, antenna #2 and antenna #3. The calculations are again based on Friis transmission equation, which in the case of two different antennas (antenna # i and antenna # j) measured during experiment # k ($k = 1,2,3$) becomes:

$$G_{i\ \mathrm{dB}} + G_{j\ \mathrm{dB}} = 20\log_{10}\left(\frac{4\pi R}{\lambda}\right) + 10\log_{10}\left(\frac{P_r}{P_t}\right)^{(k)} \tag{53}$$

5.8. The system of equations describing all three experiments is:

$$\begin{aligned} G_{1\ \mathrm{dB}} + G_{2\ \mathrm{dB}} &= 20\log_{10}\left(\frac{4\pi R}{\lambda}\right) + 10\log_{10}\left(\frac{P_r}{P_t}\right)^{(1)} \\ G_{1\ \mathrm{dB}} + G_{3\ \mathrm{dB}} &= 20\log_{10}\left(\frac{4\pi R}{\lambda}\right) + 10\log_{10}\left(\frac{P_r}{P_t}\right)^{(2)} \\ G_{2\ \mathrm{dB}} + G_{3\ \mathrm{dB}} &= 20\log_{10}\left(\frac{4\pi R}{\lambda}\right) + 10\log_{10}\left(\frac{P_r}{P_t}\right)^{(3)} \end{aligned} \tag{54}$$

5.9. The right-hand side of the equations in (54) is known after an accurate measurement is performed on the distance R, and the ratios received-power/transmitted-power. Thus, the following system of three equations with three unknowns is obtained:

$$\begin{aligned} G_{1\ \mathrm{dB}} + G_{2\ \mathrm{dB}} &= A \\ G_{1\ \mathrm{dB}} + G_{3\ \mathrm{dB}} &= B \\ G_{2\ \mathrm{dB}} + G_{3\ \mathrm{dB}} &= C \end{aligned} \tag{55}$$

5.10. The solution to the system of equations in (55) is easily found to be:

$$\boxed{\begin{aligned} G_{1\ \mathrm{dB}} &= \frac{A+B-C}{2} \\ G_{2\ \mathrm{dB}} &= \frac{A-B+C}{2} \\ G_{3\ \mathrm{dB}} &= \frac{-A+B+C}{2} \end{aligned}} \tag{56}$$

5.11. The ***gain-transfer (or gain-comparison) method*** requires an antenna whose gain is exactly known. This antenna is called ***gain standard***. Two sets of measurements are performed.

1) The test antenna is in receiving mode, and its received power P_T is measured;
2) The gain standard is in receiving mode in exactly the same arrangement (the distance R and the transmitted power P_0 are kept the same), and its received power P_S is measured.

In both measurements, the receiving antennas must be matched to their loads (the receiver).

5.12. The calculation of the test antenna gain in dB is based on Friis transmission equation. Both experiments described above lead to the following system of equations:

$$G_{T\,\mathrm{dB}} + G_{0\,\mathrm{dB}} = 20\log_{10}\left(\frac{4\pi R}{\lambda}\right) + 10\log_{10}\left(\frac{P_T}{P_0}\right)^{(1)}$$
$$G_{S\,\mathrm{dB}} + G_{0\,\mathrm{dB}} = 20\log_{10}\left(\frac{4\pi R}{\lambda}\right) + 10\log_{10}\left(\frac{P_S}{P_0}\right)^{(2)} \quad (57)$$

Here,

$G_{T\,\mathrm{dB}}$ is the gain of the test antenna;

$G_{S\,\mathrm{dB}}$ is the gain of the gain standard; and

$G_{0\,\mathrm{dB}}$ is the gain of the transmitting antenna.

5.13. From (57), one can derive the expression for the calculation of the gain of the test antenna:

$$\boxed{G_{T\,\mathrm{dB}} = G_{S\,\mathrm{dB}} + 10\log_{10}\left(\frac{P_T}{P_S}\right)} \quad (58)$$

5.14. If the test antenna is circularly or elliptically polarized, two orthogonal linearly polarized gain standards must be used in order to obtain the partial gains corresponding to each linearly polarized component. The total gain of the test antenna is:

$$G_{T\,\mathrm{dB}} = 10\log_{10}(G_{Tv} + G_{Th}), \quad (59)$$

where:

G_{Tv} is the dimensionless gain of the test antenna measured with the vertically polarized gain standard; and

G_{Th} is the dimensionless gain of the test antenna measured with the horizontally polarized gain standard.

6. Directivity measurements

6.1. The directivity measurements are directly related to the pattern measurements. Once the pattern is well defined in the 3-D space, the directivity can be determined using its definition as:

$$D_0 = 4\pi \frac{F_{\max}(\theta_0, \varphi_0)}{\int_0^{2\pi}\int_0^{\pi} F(\theta,\varphi)\sin\theta\, d\theta\, d\varphi}, \quad (60)$$

where $F(\theta,\varphi)$ is the radiation pattern of the test antenna.

6.2. Generally, the radiation pattern $F(\theta,\varphi)$ is measured by sampling the field over a sphere of constant radius R. The spacing between the sampling points depends on the directive properties of the antenna and on the desired accuracy. As discussed in LO3 and LO4, the far-field pattern can be measured directly or via NF/FF transformations. It may also be approximated by making use of the 2-D patterns measured in the three (or two) principal planes.

6.3. The integral:

$$\Pi = \int_0^{2\pi}\int_0^{\pi} F(\theta,\varphi)\sin\theta\, d\theta\, d\varphi \quad (61)$$

is usually solved numerically, e.g.:

$$\Pi \simeq \frac{\pi}{N}\frac{2\pi}{M}\sum_{j=1}^{M}\left[\sum_{i=1}^{N} F(\theta_i, \varphi_j)\sin\theta_i\right] \quad (62)$$

6.4. If the antenna is circularly or elliptically polarized, two measurements of the above type must be carried out in order to determine the partial directivities, D_θ and D_φ. Then, the total directivity is calculated as:

$$D_0 = D_\theta + D_\varphi \quad (63)$$

where the partial directivities are defined as:

$$D_\theta = 4\pi \frac{F_{\theta \max}}{\Pi_\theta + \Pi_\varphi}; \tag{64}$$

$$D_\varphi = 4\pi \frac{F_{\varphi \max}}{\Pi_\theta + \Pi_\varphi}; \tag{65}$$

7. Radiation efficiency, e_{cd}

7.1. In order to calculate the radiation efficiency, the gain and the directivity must be measured first. Factors like impedance mismatch and polarization mismatch have to be minimized during those measurements. The radiation efficiency is then calculated using its definition:

$$e_{cd} = \frac{\text{Gain}}{\text{Directivity}} \tag{66}$$

8. Impedance measurements

8.1. The input impedance of an antenna is calculated via the reflection coefficient at its terminals Γ, which are connected to a transmission line of known characteristic impedance Z_c. If the magnitude and the phase of Γ are known, then, the antenna input impedance is calculated as:

$$\boxed{Z_A = Z_c \frac{1+\Gamma}{1-\Gamma}}, \ \Omega \tag{67}$$

8.2. The magnitude of the reflection coefficient $|\Gamma|$ is found from the measurement of the SWR (Standing Wave Ratio) in the transmission line:

$$\boxed{|\Gamma| = \frac{SWR-1}{SWR+1}} \tag{68}$$

From transmission-line theory, it is known that the SWR is defined as the ratio of the maximum value to the minimum value measured along the transmission line terminated with a certain load.

8.3. The envelope of the voltage along a transmission line terminated with an unmatched load is shown below. The minima and the maxima of the voltage along the line can be clearly identified. The SWR is defined as:

$$SWR = \frac{|V|_{\max}}{|V|_{\min}} \tag{69}$$

The SWR is a number between 1 and infinity. When $SWR = 1$, a pure traveling wave exists in the transmission line, and the signal envelope is constant along the line. This mode is achieved when perfect impedance match is in place. When $SWR \to \infty$, then a pure standing wave is established in the line with the minima of the wave being exactly zero. This happens when the line is terminated with a short circuit or an open circuit.

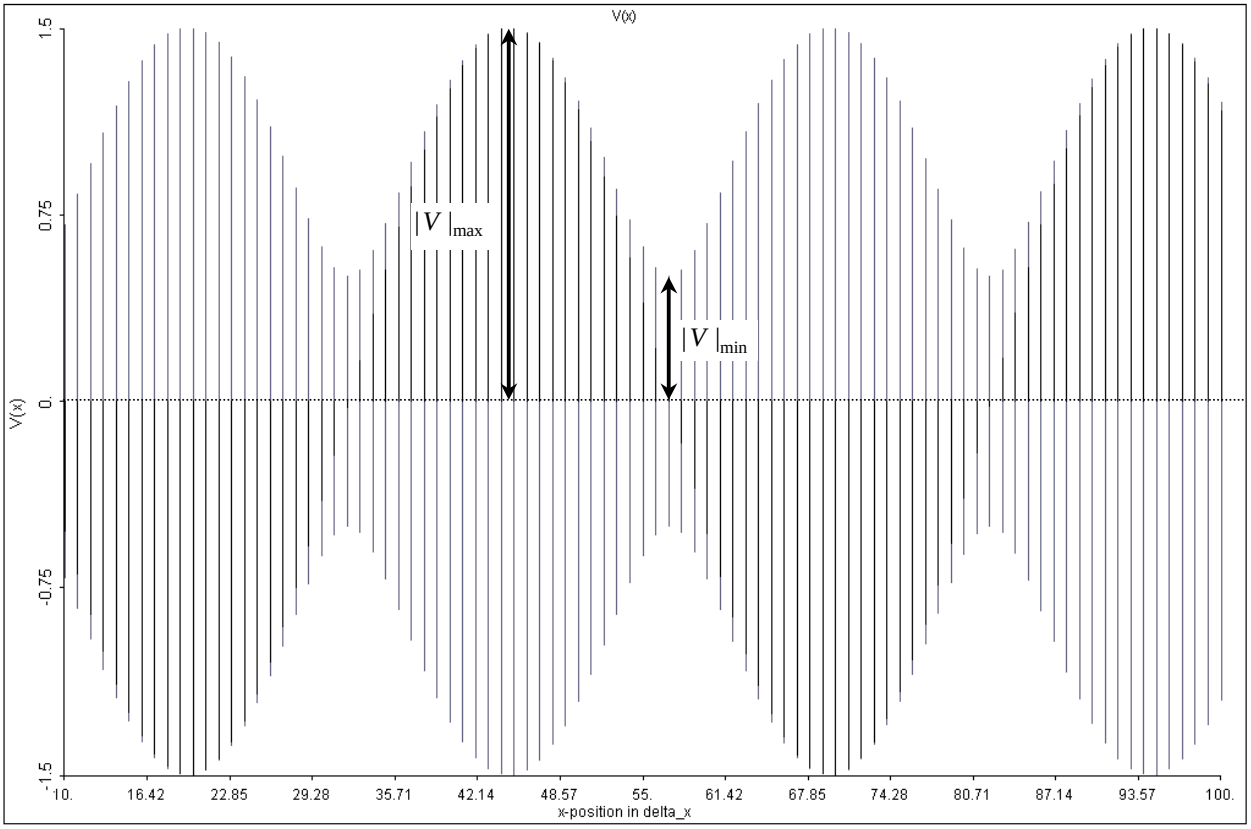

8.4. The phase of $\Gamma = |\Gamma| e^{j\gamma}$ can be determined by locating a voltage maximum or a voltage minimum in the transmission line at a certain distance x away from the antenna. The ratio of this distance and the wavelength in the line λ_g is used to calculate the phase of Γ:

$$\boxed{\gamma = 2k_g x_n \pm (2n-1)\pi = \frac{4\pi}{\lambda_g} x_n \pm (2n-1)\pi} \qquad (70)$$

Here:

n is the number of the voltage minimum as counted from the antenna terminals;

x_n is the distance from the antenna terminals to the n-th voltage minimum;

$k_g = 2\pi / \lambda_g$ is the guide (transmission line) phase constant.

8.5. Equation (70) is found by deriving the minima of the total field in the transmission line as a function of the distance from the antenna terminals x. The voltage magnitude distribution is shown in the figure below.

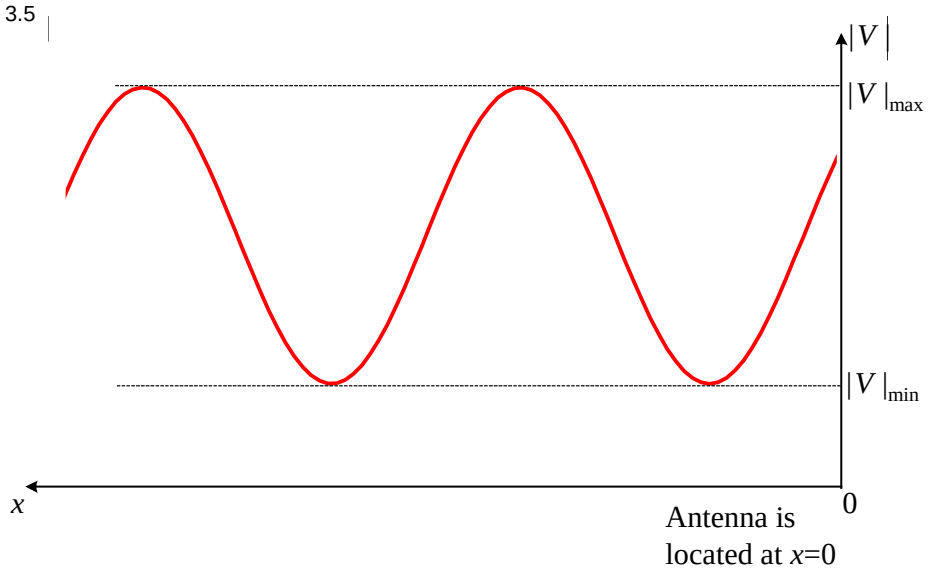

8.6. First, we have to determine the magnitude of the total voltage as a function of x. Assuming that the incident voltage is represented by the phasor:

$$\tilde{V}^i(x) = \tilde{V}^i(0)e^{+jk_g x}, \tag{71}$$

one obtains the reflected voltage as:

$$\tilde{V}^r(x) = \Gamma\tilde{V}^i(0)e^{-jk_g x} \tag{72}$$

8.7. The total voltage in the transmission line is the superposition of the incident and the reflected waves:

$$\begin{aligned}\tilde{V}(x) &= \tilde{V}^i(x) + \tilde{V}^r(x)\\ \tilde{V}(x) &= \tilde{V}^i(0)[e^{+jk_g x} + \Gamma e^{-jk_g x}] = \tilde{V}^i(0)[e^{+jk_g x} + |\Gamma|\, e^{-j(k_g x-\gamma)}]\end{aligned} \tag{73}$$

The magnitude of the voltage is determined as:

$$|\tilde{V}(x)|^2 = |\tilde{V}^i(0)|^2\,\{[\cos(k_g x) + |\Gamma|\cos(k_g x-\gamma)]^2 + [\sin(k_g x) - |\Gamma|\sin(k_g x-\gamma)]^2\} \tag{74}$$

8.8. To obtain all extrema of the function $|\tilde{V}(x)|^2$, one has to find the roots of the equation:

$$\frac{\partial\,|\tilde{V}(x)|^2}{\partial x} = 0 \tag{75}$$

Equations (74) and (75) lead to the equation:

$$\sin(2k_g x - \gamma) = 0, \tag{76}$$

whose solutions give all values of x, at which the function's extrema are found:

$$2k_g x_n = \gamma + n\pi, \quad n = 0, \pm1, \pm2, \ldots \tag{77}$$

8.9. The odd values of $n = \pm1, \pm3, \pm5, \ldots$ in (77) correspond to the minima of the function $|\tilde{V}(x)|^2$. Thus, one can formulate the equation for the calculation of γ via the location of the minima as:

$$\boxed{\gamma = 2k_g x_n \pm (2n-1)\pi, \quad n = 1, 2, 3, \ldots} \tag{78}$$

The value of n in (78) shows the number of the respective minimum as counting from the antenna (load) terminals.

9. Polarization measurements

9.1. A complete description of the antenna polarization requires an accurate description of the polarization ellipse (the axial ratio and the tilt angle), as well as the sense of rotation (clockwise, or counter-clockwise). All these concepts have already been defined in LO9.

9.2. It must be pointed out that, in general, the polarization of an antenna is not the same in every direction, i.e., it depends on the observation angle. That is why, often, a number of measurements are required according to the desired degree of polarization description.

9.3. The polarization measurement methods are classified into three general categories.

- Partial methods: they give incomplete information about the polarization but are simple and require conventional equipment.
- Comparison methods: they yield complete polarization information; however, they require a polarization standard.
- Absolute methods: they yield complete polarization information; and, they do not require a polarization standard.

9.4. One of the popular partial methods is the ***polarization-pattern method***. It produces the polarization ellipse parameters (the axial ratio and the tilt angle) in a given direction of radiation. It cannot determine however the sense of rotation. The AUT can be either in transmitting or in receiving mode. The other antenna (the probe) must be linearly polarized, e.g. a dipole, and its pattern must be accurately known.

9.5. A typical arrangement for the polarization-pattern measurement is given below.

The direction of radiation is specified by the angles (θ,φ).

9.6. The signal at the output of the probe depends on two factors: the test antenna's polarization and the angle of the probe's rotation. The signal's level is recorded and plotted versus the angle of rotation. Thus, the polarization pattern is obtained for the considered direction of radiation. There are three typical contours that can be observed: the linear polarization pattern, the circular polarization pattern, and the most general pattern of the elliptical polarization.

9.7. Let us assume that the probe is initially in such a position that it is polarized along the z-axis. If the AUT is linearly polarized along the z'-axis, where $z' \equiv z$, then the polarization pattern is a $\cos\psi$ function of the rotation angle ψ with respect to the z-axis.

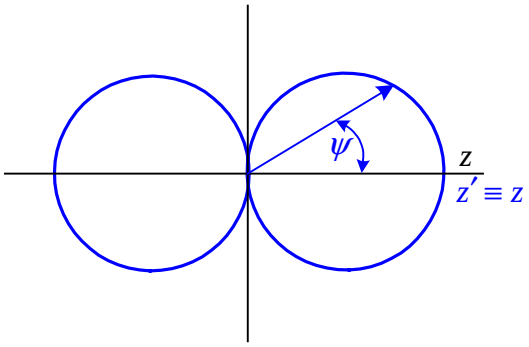

This is obvious from the fact that the PLF of two linearly polarized antennas is determined by the dot product of their polarization vectors, $PLF = |\hat{\rho}_t \cdot \hat{\rho}_r|^2$, as discussed in LO9.

9.8. Obviously, in the general linear polarization case, the polarization pattern will be tilted with respect to the polarization axis of the probe. The polarization pattern then will be $\cos(\psi - \psi_0)$, where ψ_0 is the angle between the polarization axes of both antennas for the initial orientation of the probe. However, the shape of the pattern will remain the same, indicating the linear polarization of the AUT.

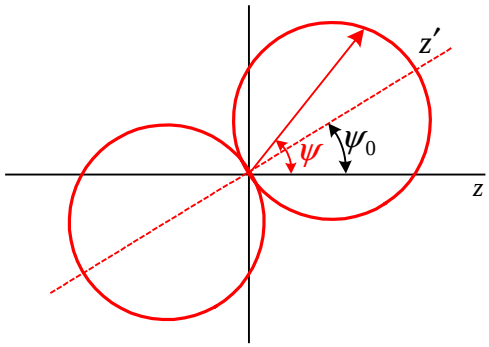

9.9. If the AUT is circularly polarized, the polarization pattern is a circle regardless of the initial mutual orientation of the probe and the AUT.

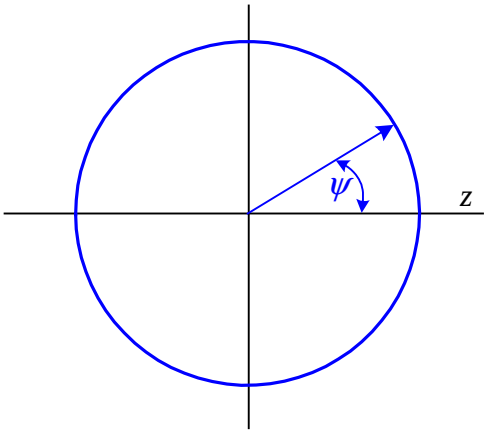

9.10. In the general case of elliptically polarized test antenna, a typical dumb-bell contour is obtained, which allows the direct calculation of the axial ratio and the tilt angle τ of the polarization ellipse as it is shown in the figure below.

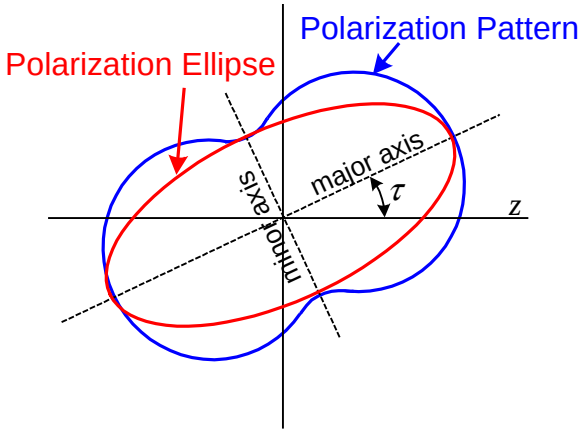

9.11. The polarization-pattern method cannot provide information about the sense of rotation of the field of circularly or elliptically polarized antennas. However, this parameter can be easily established by the use of circularly polarized probes (e.g. spiral antennas): one of a clockwise polarization, and the other one of a counter-clockwise polarization. Whichever receives a stronger signal will determine the sense of rotation.

9.12. Another partial method is the ***axial-ratio pattern method***. The arrangement is very similar to that of the polarization-pattern method. The only difference is that now the test antenna (which operates in a receiving mode, usually) is rotated in a desired plane by the antenna positioning mechanism. The probe must rotate with much larger angular frequency than the test antenna because it should complete one full turn at approximately every degree of rotation of the test antenna.

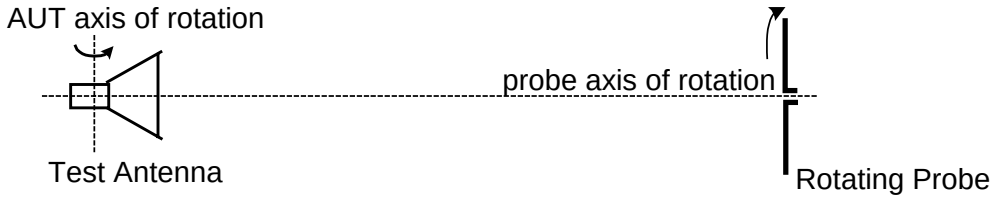

9.13. As a result of the measurement described above, a 2-D pattern is obtained, which allows the calculation of the axial ratio of the polarization at any direction of the measured 2-D pattern. Such a pattern (in dB) of a nearly circularly polarized antenna is shown below.

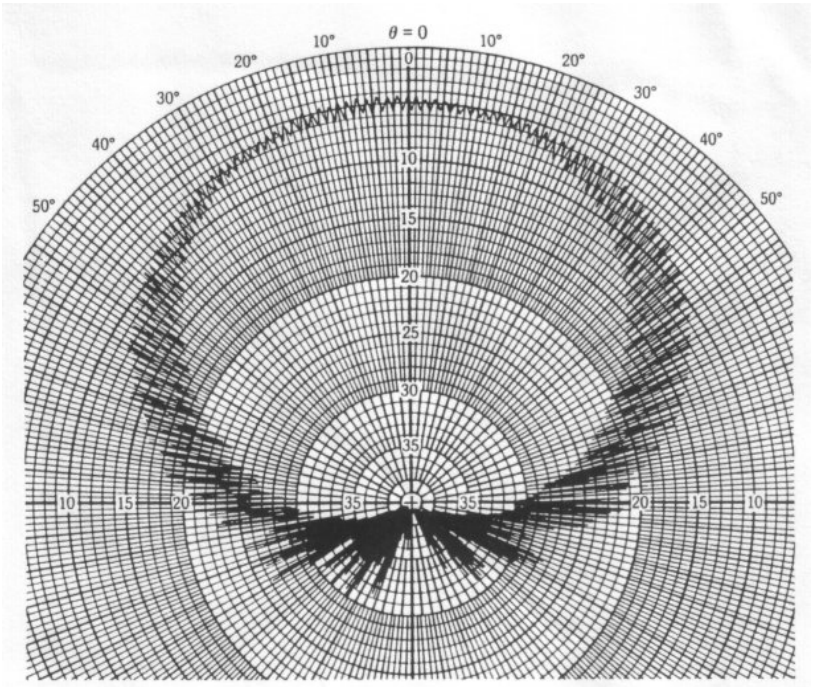

Figure 16.26 Pattern of a circularly polarized test antenna taken with a rotating, linearly polarized, source antenna [E. S. Gillespie, ''Measurement of Antenna Radiation Characteristics on Far-Field Ranges,'' in *Antenna Handbook* (Y. T. Lo & S. W. Lee, eds.), 1988, © Van Nostrand Reinhold Co., Inc.]

9.14. From the example pattern above, it is obvious that the axial ratio pattern has an inner envelope and an outer envelope. The ratio of the outer envelope to the inner one for a given angle gives the axial ratio of the E-field polarization in this direction. For example, the pattern above shows that the test antenna is nearly circularly polarized along its axis, i.e. its axial ratio is closed to one. At greater observation angles, however, its polarization becomes elliptical of increasingly large axial ratio.

9.15. The axial ratio pattern method yields only the axial ratio of the polarization ellipse. It does not give information about the tilt angle and the sense of rotation. However, it is very fast and convenient to

implement in any antenna test range. The tilt angle at selected directional angles can be always clarified later with the polarization-pattern method.

9.16. A powerful absolute polarization measurement method, which is often used in practice, is the ***three-antenna method***. The method will not be described in detail here since it involves more advanced knowledge on monochromatic EM wave polarization. The interested reader is referred to the existing extensive technical references given at the end of this module. The three-antenna method yields full polarization information for all three antennas. The only *a-priori* knowledge required is the approximate tilt angle of one of the three antennas.

9.17. The method requires the measurement of the amplitude and the phase of the normalized received voltage in three experiments, which involve: 1) antenna #1 and antenna #2; 2) antenna #1 and antenna #3; and 3) antenna #2 and antenna #3. All three experiments must use the same measurement set-up. The three complex voltage phasors are measured as a function of the angles φ and χ, which are the angles of rotation of the antennas about the antenna-range axis (usually, this is the line-of-sight between them).

9.18. The angles φ and χ show the clockwise rotation of each antenna as one looks from it towards the other antenna. An example set-up is shown in the figure below. First, the AUT#1 is scanned for $\phi \in [0^\circ, 360^\circ]$ usually with a step of $\triangle\phi = 1^\circ$. Then, the angle of AUT#2 is incremented by $\triangle\chi$ (usually, $\triangle\chi \approx 15^\circ$), and AUT#1 is scanned again. This is repeated until the angle χ sweeps the whole range from 0° to 360°.

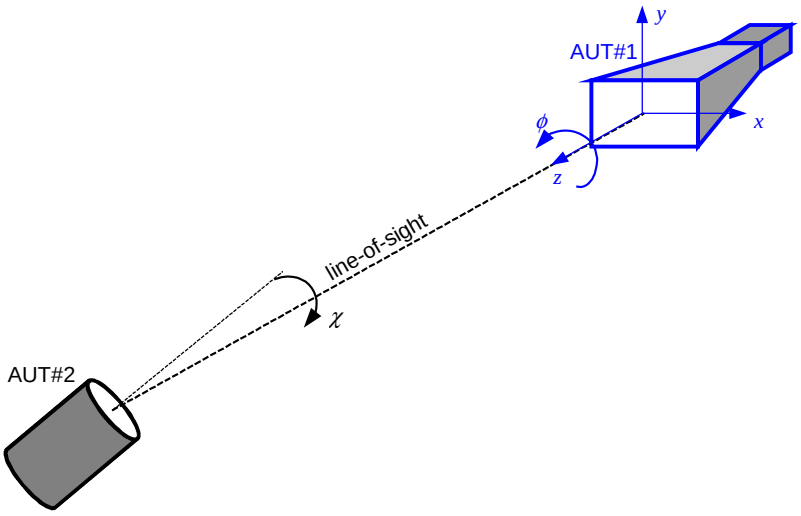

9.19. Three complex quantities M_{mn} are then calculated from the double Fourier transform of the voltage phasor patterns:

$$M_{mn} = \frac{\int_0^{2\pi}\int_0^{2\pi} \tilde{V}_{mn}(\phi,\chi) e^{+j(\phi+\chi)} d\phi d\chi}{\int_0^{2\pi}\int_0^{2\pi} \tilde{V}_{mn}(\phi,\chi) e^{-j(\varphi+\chi)} d\phi d\chi}, \quad mn = 12, \text{ or } 13, \text{ or } 23 \tag{79}$$

9.20. It can be shown (see references [6],[7],[8]) that M_{mn} are equal to the dot products of the circular polarization ratios (see reference [3]) of the two antennas used in the respective measurement:

$$\begin{aligned} \hat{\rho}_{c1} \cdot \hat{\rho}_{c2} &= M_{12} \\ \hat{\rho}_{c1} \cdot \hat{\rho}_{c3} &= M_{13} \\ \hat{\rho}_{c2} \cdot \hat{\rho}_{c3} &= M_{23} \end{aligned} \tag{80}$$

9.21. The system in (80) is used to solve for the three circular polarization ratios:

$$\hat{\rho}_{c1} = \sqrt{\frac{M_{12}M_{13}}{M_{23}}};\ \ \hat{\rho}_{c2} = \sqrt{\frac{M_{12}M_{23}}{M_{13}}};\ \ \hat{\rho}_{c3} = \sqrt{\frac{M_{23}M_{13}}{M_{12}}} \tag{81}$$

The square root of a complex number implies ambiguity in the phase calculations for the polarization vectors. Here, it becomes necessary to have an approximate knowledge of the tilt angle of one of the antennas. The circular polarization ratios are directly related to the polarization ellipse, as described in [2] and in [3].

References

[1] *IEEE Standard Test Procedures for Antennas*, IEEE Std 149-1979, IEEE Inc., 1979, distributed by Wiley-Interscience.

[2] J.S. Hollis, T.J. Lyon, and L. Clayton, Jr., *Microwave Antenna Measurements*, Scientific-Atlanta, Inc., Atlanta, Georgia, July 1970.

[3] W.H. Kummer and E.S. Gillespie, "Antenna measurements-1978," *Proc. IEEE*, vol. 66, No. 4, pp. 483-507, April 1978.

[4] C.A. Balanis, *Antenna Theory*, 2nd ed., John Wiley & Sons, Inc., New York, 1997.

[5] J. Kraus, *Antennas*, 2nd ed., McGraw Hill, Inc., New York, 1988.

[6] J.R. Jones and D.W. Hess, "Automated three-antenna polarization measurements using digital signal processing," white paper available for download at http://www.mi-technologies.com/techliterature/

[7] E.B. Joy, and D.T. Paris, "A practical method for measuring the complex polarization ratio of arbitrary antennas," *IEEE Trans. on Antennas and Propagation*, vol. AP-21, pp. 432-435, 1973.

[8] A.C. Newell, and D.M. Kerns, "Determination of both polarization and power gain of antennas by a generalised 3-antenna measurement method," Electronics Letters, vol. 7, No. 3, pp.68-70, February 11, 1971.